



UNIVERSITY OF LEEDS

This is a repository copy of *Analysis of 2D DNA Origami with Nanopipettes*.

White Rose Research Online URL for this paper:

<http://eprints.whiterose.ac.uk/133975/>

Version: Accepted Version

Article:

Raveendran, M orcid.org/0000-0003-3968-3673, Lee, AJ orcid.org/0000-0003-2268-4645, Wälti, C orcid.org/0000-0001-9286-5359 et al. (1 more author) (2018) Analysis of 2D DNA Origami with Nanopipettes. *ChemElectroChem*, 5 (20). pp. 3014-3020. ISSN 2196-0216

<https://doi.org/10.1002/celc.201800732>

© 2018 WILEY-VCH Verlag GmbH & Co. KGaA, Weinheim. This is the peer reviewed version of the following article: Raveendran, M., Lee, A., Walti, C. and Actis, P. (2018), Analysis of 2-D DNA origami with nanopipettes. *ChemElectroChem*, doi:10.1002/celc.201800732, which has been published in final form at <https://doi.org/10.1002/celc.201800732>. This article may be used for non-commercial purposes in accordance with Wiley Terms and Conditions for Self-Archiving. Uploaded in accordance with the publisher's self-archiving policy.

Reuse

Items deposited in White Rose Research Online are protected by copyright, with all rights reserved unless indicated otherwise. They may be downloaded and/or printed for private study, or other acts as permitted by national copyright laws. The publisher or other rights holders may allow further reproduction and re-use of the full text version. This is indicated by the licence information on the White Rose Research Online record for the item.

Takedown

If you consider content in White Rose Research Online to be in breach of UK law, please notify us by emailing eprints@whiterose.ac.uk including the URL of the record and the reason for the withdrawal request.



eprints@whiterose.ac.uk
<https://eprints.whiterose.ac.uk/>

Analysis of 2-D DNA Origami with Nanopipettes

Mukhil Raveendran, Dr. Andrew J. Lee, Prof. Dr. Christoph Wälti, Dr. Paolo Actis
Pollard institute, School of Electronic and Electrical Engineering, University of Leeds, Leeds,
United Kingdom

Abstract:

Nanopipettes are a useful tool for the detection and analysis of biological molecules at the single molecule level. Here we employ nanopipettes fabricated from glass capillaries to identify two differently structured 2D DNA origami via the distinctive amplitude and dwell time of the ion current peak resulting from the translocation of the origami through the nanopipette pore. We demonstrate that the ion current peak originating from frame-like DNA origami comprises two individual peaks in contrast to solid tiles of similar size which only lead to a single peak in the ion current. Interestingly, the fine details of the shape of the double peak characteristic of the translocation of DNA origami frames are correlated with the structural features of the DNA origami. In particular, the size of the central cavity governs the lag time between the two constituent peaks of the double-peak. In summary, this work demonstrates the ability of glass nanopipettes to identify and characterize differently structured DNA origami of similar size, advancing the potential of nanopipettes for high sensitivity single molecule studies.

Introduction:

Nanopipettes are a class of nanopores fabricated from glass capillaries which have been employed for the detection, analysis, and manipulation of single molecules in solution^[1–4]. Such nanopipettes can be readily fabricated at the bench with tunable and highly controlled pore sizes ranging from a few micrometres down to 20 nm in diameter^[5,6], making them a cost effective alternative to traditional solid state nanopores. The detection and analysis of single molecule with nanopipettes relies on the principle of resistive pulse sensing^[7]. For this, the nanopipette is filled with and the tip immersed in an electrolyte and a voltage is applied between an electrode inside and an electrode outside of the nanopipette to generate an electric field at its tip^[8–10]. This field drives the molecule of interest through the nanopipette pore, which, if is of similar size as the Stokes diameter of the molecules, results in a short but easily detectable pulse in an otherwise steady ionic current^[7,11,12]. The single-molecule sensitivity of this approach has led to the adoption of nanopipettes in many label-free and carrier-based single biomolecule detection, delivery and bio-sensing applications.

The application of nanopipettes as single molecule sensors has received considerable attention recently, and in particular the detection of complex DNA folding regimes^[13] and proteins^[4] have been demonstrated. Moreover, the adaptation of the nanopipette with a DNA origami “gate” structure has been shown to enable the orchestration of controlled DNA translocation^[14]. Furthermore to enable selective single molecule sensing with high sensitivity, Keyser et al developed a DNA carrier-based antibody detection technique using DNA nanostructures which combine antigen presentation alongside a unique barcode identifier made up of dumbbell hairpin protrusions^[15]. An alternative strategy for single molecule sensing employed by Edel et al involved protein detection using nucleic aptamer-modified DNA carriers^[16] and DNA aptamer-functionalized gold nanoparticles^[17]. Using a different approach, Long et al showed that nanopipettes can be employed for label- and carrier-free detection of individual immune-complexes^[18]. This body of work illustrates that DNA conjugates and carriers, nanoparticles and aptamers can increase the sensitivity and signal for selective detection of molecules using nanopipettes. Building on this, it can be argued that DNA nanostructures – particularly DNA origami – have even greater potential to enhance single molecule detection in conjunction with nanopipettes owing to their compact size while offering a uniquely addressable carrier.

DNA origami is a nanoscale self-assembly technique that uses a set of short DNA oligonucleotide (“staples”) to fold a long single-stranded DNA (ssDNA – “scaffold”) into arbitrarily designed structures^[19,20]. Since its inception, a large range of 2D and 3D nanostructured DNA origami with varying complexity including solid and wireframe geometries and with a range of applications in nanoelectronics and nanophotonics^[19,21], as drug delivery platforms, molecular breadboards to host and control individual enzymes for direct single molecule studies using high speed atomic force microscopy^[22], and single molecule detection systems using the DNA origami as a nanopore^[23,24], inter alia, have been demonstrated.

Recently, the translocation of such DNA nanostructures through nanopores has been investigated. In particular, the differentiation of DNA cubes from RNA rings was demonstrated using variations of the peak dwell time and the peak ion current through a 50 nm silicon nitride nanopore membrane^[25]. Similarly, Zhu et al used nanopipettes to detect double helix concatamers and examined the translocation dwell time to extract information on their length and folding state^[26]. Further work using DNA origami as a molecular breadboard to isolate nuclear pore complexes enabled the differentiation between wild type and mutant forms by analysis of their characteristic ion current traces^[27].

However, despite these remarkable successes, the relationship between the structure of the DNA origami and the corresponding ion current during translocation remains largely unexplored, which hinders the adoption of DNA origami as carrier and unique identifier in nanopipette applications. In this work, we demonstrate that glass nanopipettes with sub-100-nm-pore diameters are capable of detecting structural and geometrical differences between different DNA origami (Figure 1). In particular, we show that the shape of the translocation-induced ion current peak can be used as a fingerprint to distinguish frame-shaped from solid tile-shaped DNA origami.

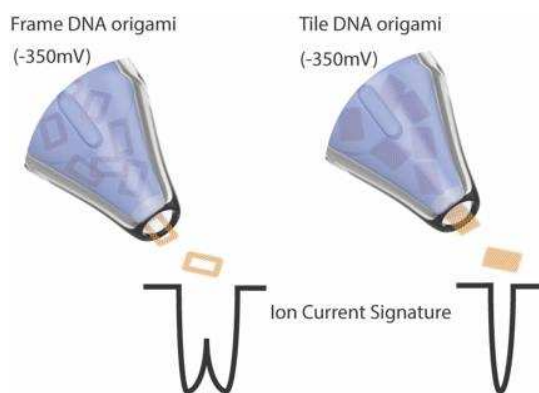


Figure 1 The top panel shows a schematic representation of the nanopipette for translocating ‘Frame’ (left) and ‘Tile’ (right) DNA origami. The bottom panel indicates the corresponding ion currents during DNA origami translocation.

Results and Discussion:

We have investigated the behaviour of four different DNA origami of similar size to understand if the structural differences in DNA origami correlated with the ion current signals. The four origami designs, two frame structures (F1 and F2) and two solid tile structures (T1 – plain tile and T2 – same as T1 tile but with additional protruding loops), were formed through different folding of an identical ssDNA scaffold (see supplementary information). Importantly, the plain tile and frame DNA structures differ only in geometry and not their constituent sequence, and as a consequence their charge and molecular weights remain identical, hence any differences in the observed ion currents are directly related to the structural variation of the DNA origami and not a change in mass or charge.

The successful assembly of DNA origami folding from an M13mp18 ssDNA scaffold following previous reports [16,18] was confirmed by atomic force microscopy (AFM). Figure 2 shows representative examples of all four assembled DNA origami structures. The observed sizes are in excellent agreement with the designed dimensions for both frame and tile origami. Frame 1 (F1) is approximately 80 nm x 80 nm with an internal void of 40 nm x 40 nm, and frame 2 (F2) is ~80 nm x 100 nm with a 40 nm x 60 nm internal void (figure 2a). In comparison, both DNA tile designs, solid tile 1 (T1 – plain tile) and tile 2 (T2), are approximately 40 nm x 40 nm and differ only in that T2 contains 44 small protruding loops (figure 2b and figure S5).

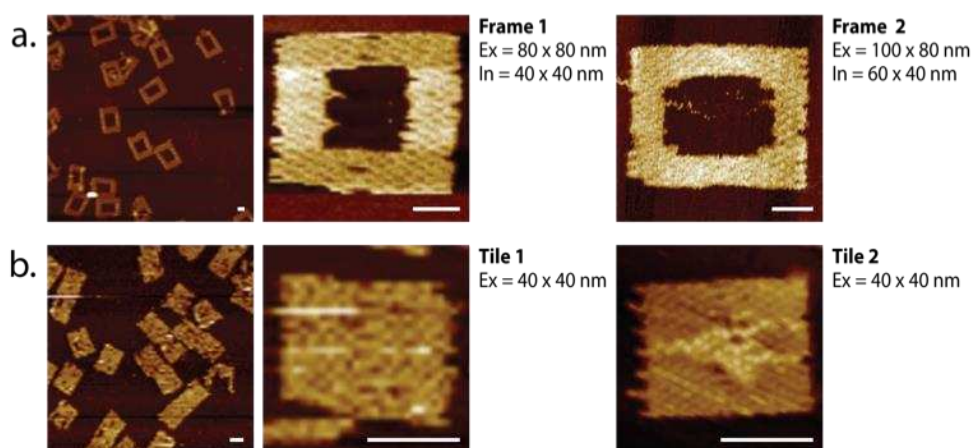


Figure 2 AFM micrographs of the different DNA origami structures showing a range of uniformly formed structures along with an individual representative AFM scan of both frame and both tile DNA origami. (a) Frame DNA origami F1 and F2 with the internal (In) and external (Ex) dimensions indicated; (b) Tile DNA origami T1 and T2 with external dimensions indicated. The scale bars for all images are 20 nm.

Nanopipettes were fabricated from quartz glass capillaries as described in the experimental section, with nanopore sizes ranging from 80 nm – 100 nm. The pore sizes were characterized indirectly via IV measurements (figure 3a) and were in good agreement with scanning electron microscopy (SEM) measurements (figure 3b). Detailed information for nanopipette pore size calculations via IV measurements are reported in the supporting information (figure S1).

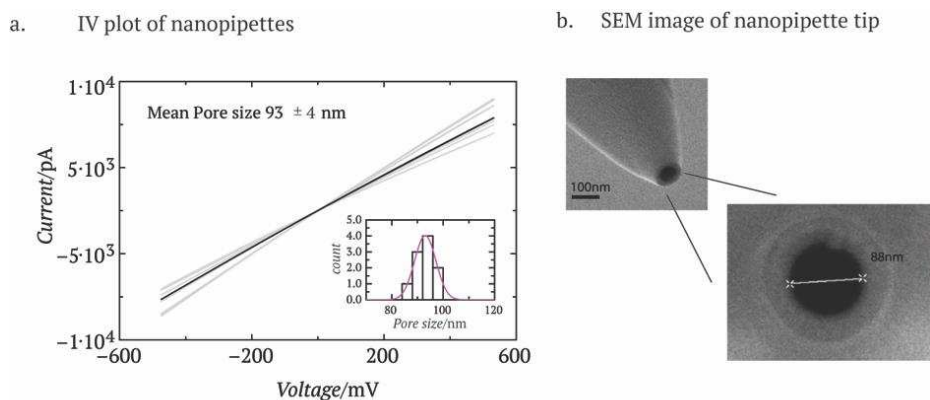


Figure 3 a. IV measurements for 10 representative nanopipettes in 0.1M KCl. The inset shows the pore size distribution obtained via IV measurements fitted with a Gaussian curve to a mean of 93 nm. b. Birds eye view and an inclined angle SEM image of the twin of one of the nanopipette from panel (a) with an IV-measured pore size of 92nm; the pore-size as measured directly by SEM (88nm) is in good agreement with the indirectly measured value.

For the translocation experiments, the nanopipettes were filled with a solution of 0.1M KCl/0.01% Tween-20 containing 500 pM of the DNA origami. A voltage of -350mV was applied between the electrode inside the nanopipette and the electrode in the surrounding electrolyte to translocate the origami through the apex of the nanopore. The translocation of the origami causes a temporary increase in the absolute value of the ionic current has been shown previously by us and others^[29–31] and it is likely due to positively charged counterions that shield the negatively charged phosphate backbone of the DNA nanostructure. Also, the increase in absolute ion current observed for our DNA origami is in good agreement with previous DNA translocation studies at salt concentrations similar to the one used here^[32]. The ion current was sampled at a rate of 100 kHz and low-pass-filtered at 20 kHz. Figure 4a shows representative examples of ion current traces representing more than 90 single molecule events obtained for each of the DNA origami structures, and figure 4b shows a selection of zoomed-in current peaks for the different origamis. Interestingly, noteworthy differences can be seen between the respective peak current amplitudes and dwell times of the translocation events of the four origami samples.

From Figure 4c, which displays the frequency of observed peak ion current amplitudes for the different origamis, it can be seen that the ion current observed during the translocation of F2, which is slightly larger in dimension than F1 (100 nm x 80 nm vs 80 nm x 80 nm), exhibit a higher mean absolute current amplitude of 59 ± 15 pA compared to 37 ± 10 pA. In contrast, both the solid tile origami T1 and T2 show a higher mean absolute current amplitude of 65 ± 11 pA and 75 ± 10 pA, respectively, than either of the frame origami structures. This may suggest that the counterion distribution of the tile origami differs from that of the frame origami, thus increasing ion flux and respective current when compared to their frame counterparts. The small difference in current amplitude between T1 and T2 might stem from the fact that T2 contains additional DNA loops on its surface which may impact on the counterion distribution and thus lead to a further increase in ion transport during translocation (figure 4c). Considering that F1, F2 and T1 DNA origami are formed from the same ssDNA scaffold and hence possess the same charge, it is noteworthy that the geometry of the origami appears to play an important role in the translocation ion current. These results corroborate the results of a recent study by Alibakhshi et al^[25] wherein the ability of silicon nitride nanopores to differentiate ring-shaped RNA and cube-shaped DNA nanoparticles using similar means was demonstrated.

Similar to the differences in mean peak current amplitude, significant differences in the dwell times of the translocation events of the different DNA origami are also observed. Figure 4d shows a frequency plot of translocation events vs dwell time. The mean of the observed dwell time for both T1 (0.08 ms) and T2 (0.07 ms) are slightly smaller than that of the frame origami F1 (0.10 ms), and much smaller than that of frame origami F2 (0.21 ms). The dwell time provides an indication of how long the DNA origami spends in the nanopore, and can therefore be used as an indicative measure of the speed of translocation. Hence, the mean dwell times of the different origami suggest that the tiles travel through the nanopipette opening faster than both frames. We note that the distribution of dwell times observed for the different DNA origami structures are significantly narrower than those found in previous studies with DNA nanostructures^[25], DNA concatemers^[26], and DNA origami^[27], where prolonged dwell times were reported. However, the nanopores employed for this work differ significantly from the ones in the cited studies and hence the results are not directly comparable.

Furthermore, a significant difference in the distribution of the translocation events with respect to current peak amplitude and dwell time can be seen between the two types of origami. Figure 4e shows a colour map of the frequency of events for the different origami, and it can be seen that the distributions for both frame origami are wider than those of the tile origami.

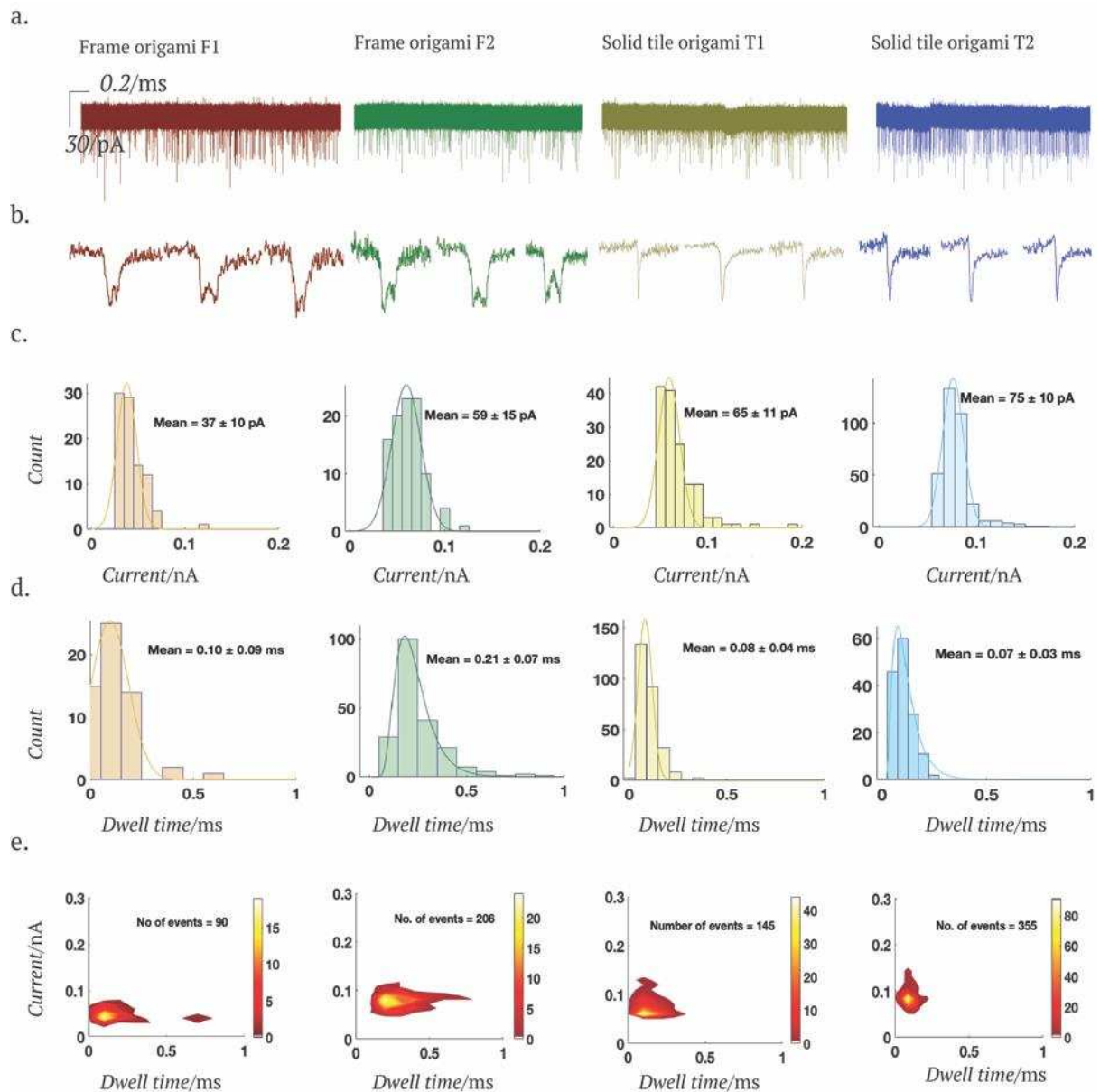


Figure 4 a. Ion current recordings for each of the frame and solid tile origami samples. The recordings are of approximately 100 seconds in duration, sampled at 100 kHz and low-pass filtered at 20 kHz to remove high-frequency noise. b. Representative selection of current peaks observed for individual translocation events for the frame and tile origami. c. Frequency of observed peak currents for each origami. The solid lines represent Gaussian fits from which the respective mean currents are obtained. d. Frequency of observed dwell times for each origami. The solid lines represent Gaussian fits from which the respective mean dwell times are obtained. e. Colour-map displaying the frequency of events with different translocation current amplitudes/dwell times, revealing that wider distributions are observed for the frame origami compared to the tile origami.

In addition to the differences in mean current peak amplitude and dwell time between the different DNA origami, it can be seen from the selection of current peaks shown in figure 4b that a distinct difference in peak shape is observed between the frame and tile origami, and we thus postulate that the peak shape can be used as a unique fingerprint of the origami to deduce small structural changes between differently folded DNA origami. Here, the tile origami was found to produce a single peak upon translocation, as would be expected for a single entity passing through the nanopore. However, where the frame structures were translocated, a characteristic double peak, or 'W'-shaped peak, was observed. The absence of such double peaks in any of the tile origami samples suggests that the double peaks are characteristic of the frame structure, and likely specifically of the presence of a void in the structure's centre. Zhang et al showed that a characteristic double peak could also appear because of tumbling of individual nanostructures during translocation [28]. An array of representative peak shapes obtained from translocation events of the frame and tile origami are provided in the supporting information (figure S6 and S7).

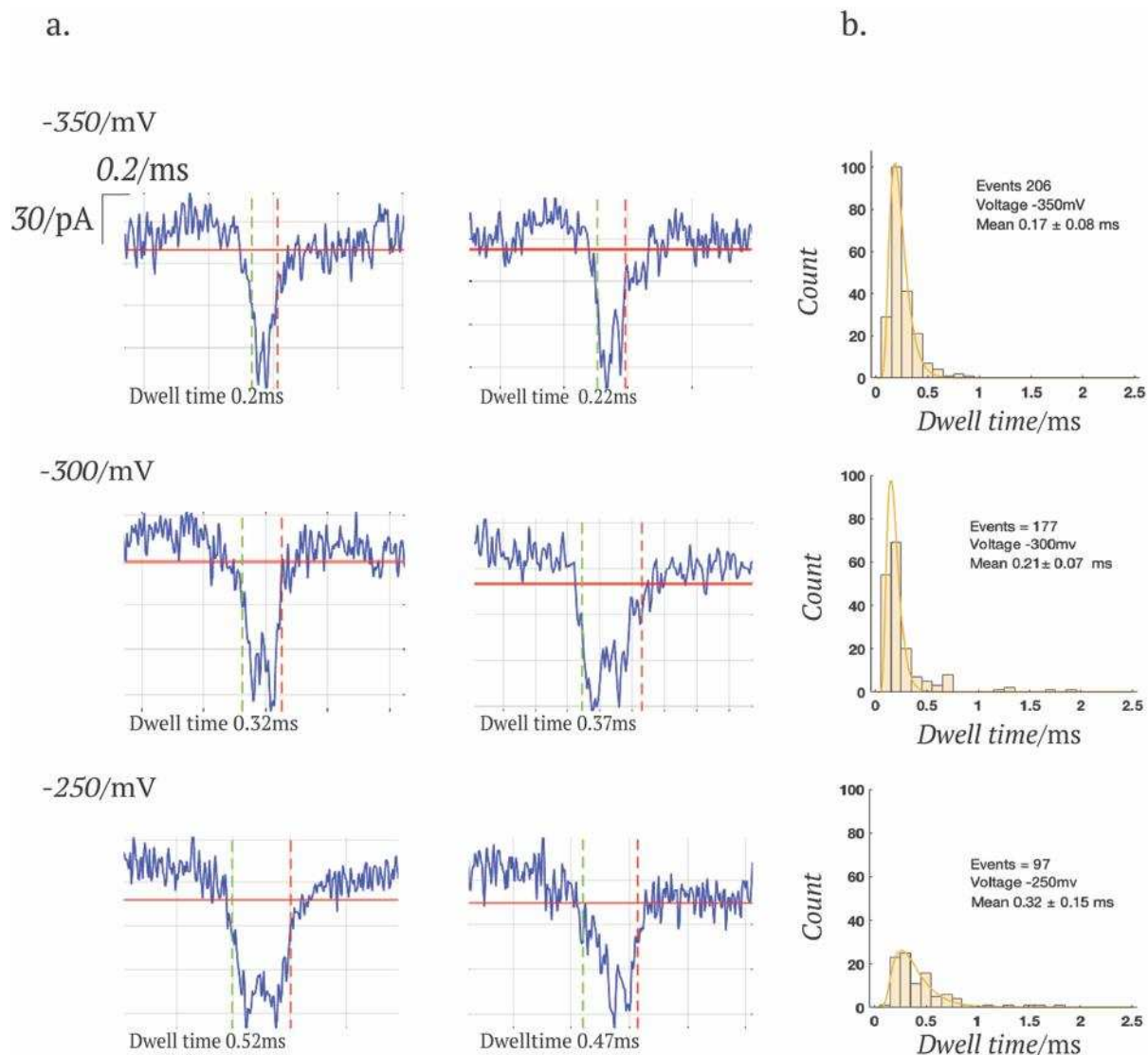


Figure 5 a. Representative set of translocation current peaks for frame origami F1 at different applied translocation voltages. The dwell times of the different peaks are indicated in the figure. It can be seen that double peaks are observed for all applied voltages. b. Frequency of dwell times for translocation of frame origami F1 at different translocation voltages; a wider distribution of dwell times is observed at lower translocation voltages, and an increase in the frequency of events is observed with increasing translocation voltage.

Using the same setup as above, translocation of DNA origami was investigated at different translocation voltages (-250 mV and -300 mV in addition to the -350 mV reported above). Figure 5a shows a number of different translocation peaks of frame origami F1 at the different translocation voltages, and it can be seen that double-peak structures are observed for all investigated translocation voltages. The dwell times of the individual translocation events are indicated in the panels, and a notable increase is observed with decreasing translocation voltage. This is corroborated by the frequency plots of events vs observed dwell time for the different translocation voltages (figure 5b). Given that the translocation of the DNA origami is driven by the applied voltage, it can be expected that the translocation speed decreases with voltage and therefore the origami will spend more time in the nanopore, resulting in an increase in observed dwell time. Similarly, the number of observed events per unit time decreases with applied translocation voltage, and while at a translocation voltage of -250 mV still a significant number of events is observed, at -200 mV, no translocation events were registered. In contrast, increasing the translocation voltage to greater than -350 mV resulted in very high translocation speeds and consequently a rapid flux of DNA origami through the nanopipette pore leading to clogging of the pore and eventually termination of the transport.

The slower translocation speed at the lower translocation voltages is also expected to improve our ability to resolve potential double-peaks, and this is indeed reflected in our data, where more prominent double-peaks are observed at lower translocation voltages.

Interestingly, the shape of the composition of the double peaks differs for the two different frame origami F1 and F2. Figure 6a shows the distribution of the dwell times of the two constituent peaks P1 and P2 of the characteristic double peaks observed during the translocation of frame origami. While the dwell time for P2 is similar for origami F1 and F2, the lag time between the two constituent peaks P1 and P2 – determined by the time difference between the occurrence of the maxima of the two peaks – has been measured, and the results for both frames are shown in figure 6b. Given that the occurrence of the double peak is linked to the frame-like shapes of the DNA origami, it can be argued that the double peak arises as a consequence of the passage of one arm of the frame through the nanopipette pore, giving rise to P1, followed by the central void, and finally the other arm of the frame, giving rise to P2. Therefore, the lag time between P1 and P2 would be related to the dimensions of the internal cavity of the frame. Indeed, the lag time for frame F2 which has a central void of 60 nm x 40 nm is almost twice as long as the that of F1 which has a smaller central void of 40 nm x 40 nm.

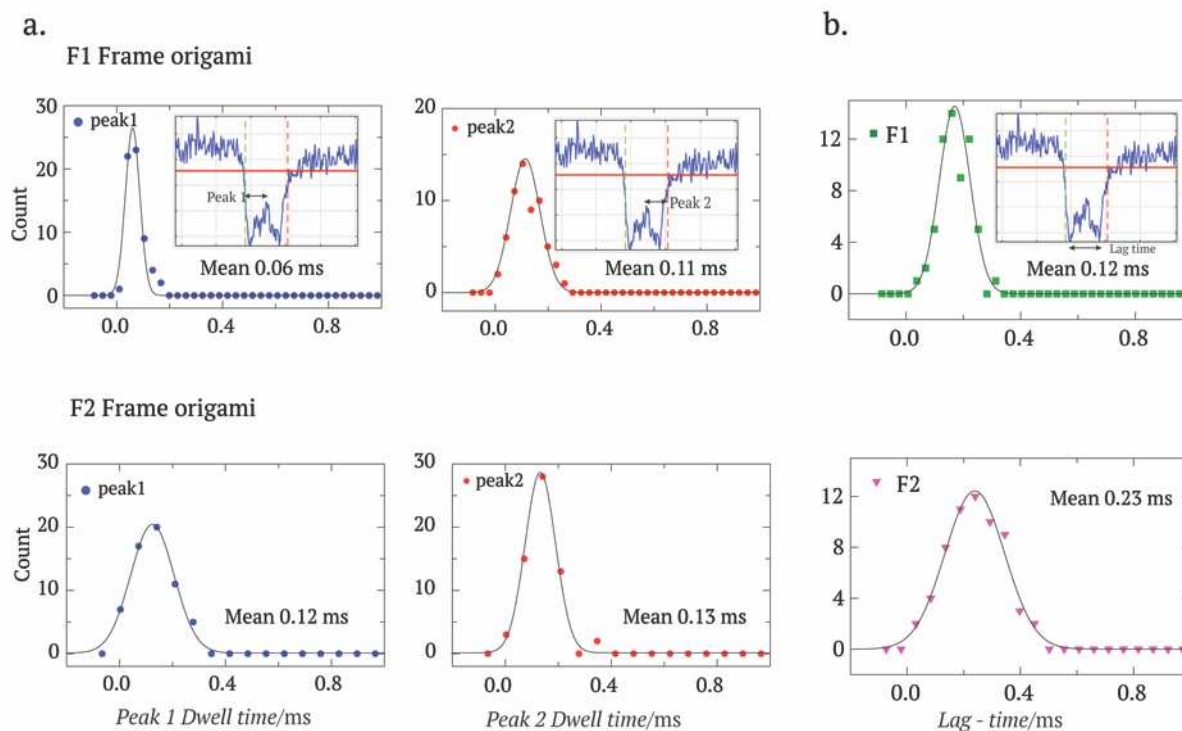


Figure 6 Dwell as lag-time analysis of the double peaks of the frame DNA origami. a. Frequency plot of the individual dwell times for individual peaks P1 and P2 for F1 (top panel) and F2 (bottom panel); the insets show a typical double peak with peak 1 and peak 2 dwell time indicated, respectively. b. Frequency plot showing the number of observed translocation events with different lag-times for frame origami F1 (top) and F2 (bottom); the inset depicts the lag-time between peak 1 and peak 2 of a typical peak. The solid lines represent Gaussian fits to the data, and the observed mean values as extracted from the fit are given in the individual panels.

Moreover, in addition to an overall longer lag time, the distribution of observed lag times for F2 ($0.23 \pm 2\%$) is significantly broader than that for F1 ($0.12 \pm 2\%$). We speculate that this may be a consequence of the symmetry of the central cavity. F1 has a symmetrical central cavity (40 nm x 40 nm), resulting in a tight distribution of double peak lag times as the relevant cavity dimension is independent of the orientation with which it travels through the nanopore. In contrast, F2 has an asymmetric cavity (40 nm x 60 nm) which would give rise different lag times depending on the direction of travel and hence to a broader distribution of lag times. This suggests that the ion currents observed during the translocation of DNA origami through nanopipette pores can be used to distinguish not only coarse structural differences (frame from tile) but also more subtle variation such as small differences in the central cavity.

Conclusion:

We have demonstrated the ability of glass nanopipettes to detect structural differences between different DNA origami, in particular to distinguish different 2D origami structures (frame from tile), which shows that nanopipettes can be employed as a highly sensitive molecular detection tool. Specifically, we have shown that both the dwell time as well as the amplitude of the ion current peak can be used to differentiate nanostructures of different types, which is in line with previous studies. In addition, we have demonstrated that structure of the peak can be used to distinguish different DNA origami structures.

The observation that the structure of the ion current peak holds sufficient information to be correlated to a particular DNA origami structure was established through the investigation of different frame and tile DNA origami structures. We found that the frame DNA origami led to a characteristic double peak, while the solid tile origami only led to single peaks in ion current. Furthermore, we provided preliminary evidence that the shape and composition of the double peak and the individual constituent peaks are related to the dimension of the frame and in particular that the lag time of between the two constituent peaks varies with the dimension of the central cavity of the frame. However, further investigations are necessary to establish fully the relationship between the detailed structure of the ion current peak and the structure and shape of the DNA origami frame.

Experimental section:

Nanopipette Fabrication and Ion-Current Measurements:

The nanopipettes were fabricated from glass capillaries (QF100-50-7.5, World precision Instruments, UK) of 0.5 mm inner diameter using a Sutter instrument model P-2000 laser puller using the pulling parameters given in the supplementary information. The resultant nanopipettes were characterised by SEM (Leo 1530 FEG-SEM) and were found to have pore diameters ranging from 80–100 nm. The observed diameters correlated well with the diameters calculated from the IV measurements. For the translocation experiments the nanopipettes were filled with 0.1M KCl and 0.01% Tween 20, pH 7.2 containing 500pM DNA origami. The tips of the nanopipettes were then immersed in 0.1M KCl with Ag/AgCl electrodes connecting the inside of the nanopipette to the outer electrolyte solution. The counter electrode was grounded and on application of a negative potential to the working electrode inside the nanopipette, DNA origami from inside the nanopipette translocate out into the electrolyte solution and the resulting current events are recorded. The presence of tween in the sample buffer allowed for the DNA origami to translocate the nanopipette readily with high event frequencies.

Ion current data were acquired using an Axon instruments-patch clamp systems (Molecular devices, USA). Measurements were recorded using the Axopatch 700b amplifier, and the data were acquired at a rate of 100 kHz, and using a 20 kHz low pass filter. The data were analyzed using MATLAB.

SEM imaging:

The laser pulled nanopipettes were imaged with a scanning electron microscope (Leo 1530 FEG-SEM) to determine the geometry of the pipette tip and to check the reproducibility of the fabrication process. The nanopipettes were coated with a gold layer of few nanometre thickness via sputter coating to reduce charging during SEM imaging. The nanopipettes were then mounted horizontally on a single stub of the sample holder using double sided carbon tape and the stage was tilted to an angle of 60 and above for imaging. The pipettes were imaged at between 2 and 3 kV at a working distance of 5 mm and below at an aperture size of 30.00m using a InLens detector.

AFM sample preparation and scanning:

All DNA origami samples were imaged using a Dimension Fastscan (Bruker, Santa Barbara, CA, USA) in tapping mode in aqueous buffer using Fastscan D Si₃N₄ cantilevers containing an Si tip. All probes were driven at resonance (110 kHz in liquid) with a typical amplitude of 10 nm. Images were acquired with a typical scan rate of 20 Hz (256 x 256 pixels). The DNA origami samples were deposited on freshly cleaved mica which had been pre-incubated with 10 mM NiCl₂ and incubated at room temperature for 10-15mins. The remaining liquid was rinsed off and topped up with a buffer containing 10 mM Tris(OAc)₂ and 10 mM Mg(OAc)₂ for imaging.

DNA origami design and folding:

All the DNA origami samples were designed using caDNA software^[33]. Scaffold routing diagrams are provided in supporting information (figure S2, S3, S4 and S5). All the staple oligonucleotide sequences used are available upon request. The DNA origami was folded by thermal annealing from a mixture M13mp18 ssDNA (New England Biolabs, MA, USA) as a scaffold and a tenfold excess of >200 short oligonucleotide staples (IDT, Coralville, IA, USA) in a buffer containing 10mM Tris(OAc)₂ (pH 7.4), 10mM Mg(OAc)₂ and 1mM EDTA (Sigma Aldrich, USA). Assembled structures were purified by removal of unincorporated staples using a Sephacryl S400 (GE healthcare, UK) size exclusion matrix in the same folding buffer.

Acknowledgements:

The authors thank Aleksandar P. Ivanov and Joshua B. Edel for generously providing and assisting with the MATLAB script, Masayuki Endo for his support with DNA origami frame design, and Mark Rosamond for the support with SEM imaging. M.R would also like to acknowledge the University of Leeds for the financial support via the Leeds Annual Research Scholarship (LARS) – PhD Scholarship.

Keywords: DNA nanotechnology, DNA origami, nanopipette, nanopore, single-molecule analysis

References:

- [1] X. Gong, A. V. Patil, A. P. Ivanov, Q. Kong, T. Gibb, F. Dogan, A. J. Demello, J. B. Edel, *Anal. Chem.* **2014**, 86, 835–841.
- [2] A. P. Ivanov, P. Actis, P. Jönsson, D. Klenerman, Y. Korchev, J. B. Edel, *ACS Nano* **2015**, 9, 3587–3594.
- [3] T. R. Gibb, A. P. Ivanov, J. B. Edel, T. Albrecht, *Anal. Chemistry* **2014**, 86, 1864–1871.
- [4] W. Li, N. A. W. Bell, S. Hernández-Ainsa, V. V. Thacker, A. M. Thackray, R. Bujdoso, U. F. Keyser, *ACS Nano* **2013**, 7, 4129–4134.
- [5] D. Perry, D. Momotenko, R. A. Lazenby, M. Kang, P. R. Unwin, *Anal. Chem.* **2016**, 88, 5523–5530.
- [6] J. Y. Y. Sze, S. Kumar, A. P. Ivanov, S.-H. Oh, J. B. Edel, *Analyst* **2015**, 140, 4828–34.
- [7] Y. Song, J. Zhang, D. Li, *Micromachines* **2017**, 8, 1–19.
- [8] L. Ying, S. S. White, A. Bruckbauer, L. Meadows, **2004**, 86, 1018–1027.
- [9] C. A. Morris, A. K. Friedman, L. A. Baker, *Analyst* **2010**, 135, 2190.
- [10] L. Shi, A. Rana, L. Esfandiari, *Sci. Rep.* **2018**, 1–12.
- [11] S. M. Oja, Y. Fan, C. M. Armstrong, P. Defnet, B. Zhang, *Anal. Chem.* **2016**, 88, 414–430.
- [12] W. J. Lan, D. A. Holden, B. Zhang, H. S. White, *Anal. Chem.* **2011**, 83, 3840–3847.
- [13] L. J. Steinbock, O. Otto, C. Chimere, J. Gornall, U. F. Keyser, *Nano Lett.* **2010**, 10, 2493–2497.
- [14] S. Hernández-Ainsa, N. A. W. Bell, V. V. Thacker, K. Göpfrich, K. Misiunas, M. E. Fuentes-Perez, F. Moreno-Herrero, U. F. Keyser, *ACS Nano* **2013**, 7, 6024–6030.
- [15] N. A. W. Bell, U. F. Keyser, *Nat. Nanotechnol.* **2016**, 11, 1–28.
- [16] J. Y. Y. Sze, A. P. Ivanov, A. E. G. Cass, J. B. Edel, *Nat. Commun.* **2017**, 8, 1–10.
- [17] X. Lin, A. P. Ivanov, J. B. Edel, *Chem. Sci.* **2017**, 8, 3905–3912.
- [18] R. J. Yu, Y. L. Ying, Y. X. Hu, R. Gao, Y. T. Long, *Anal. Chem.* **2017**, 89, 8203–8206.
- [19] P. W. K. Rothmund, *Nature* **2006**, 440, 297–302.
- [20] P. W. K. Rothmund, *IEEE/ACM Int. Conf. Comput. Des. Dig. Tech. Pap. ICCAD* **2005**, 2005, 470–477.
- [21] P. Wang, T. A. Meyer, V. Pan, P. K. Dutta, Y. Ke, *Chem* **2017**, 2, 359–382.
- [22] A. J. Lee, M. Endo, J. K. Hobbs, C. Wälti, *ACS Nano* **2018**, 12, 272–278.
- [23] N. A. W. Bell, C. R. Engst, M. Ablay, G. Divitini, C. Ducati, T. Liedl, U. F. Keyser, *Nano Lett.* **2012**, 12, 512–517.
- [24] S. Howorka, *Nat. Nanotechnol.* **2017**, 12, 619–630.
- [25] M. A. Alibakhshi, J. R. Halman, J. Wilson, A. Aksimentiev, K. A. Afonin, M. Wanunu, *ACS Nano* **2017**, 11, 9701–9710.
- [26] Z. Zhu, Y. Zhou, X. Xu, R. Wu, Y. Jin, B. Li, *Anal. Chem.* **2018**, 90, 814–820.
- [27] P. Ketterer, A. N. Ananth, D. S. Laman Trip, A. Mishra, E. Bertolin, M. Ganji, J. Van Der Torre, P. Onck, H. Dietz, C. Dekker, *Nat. Commun.* **2018**, 9, 1–8.
- [28] Y. Zhang, M. A. Edwards, S. R. German, H. S. White, *J. Phys. Chem. C* **2016**, 120 (37), 20781–20788
- [29] L. J. Steinbock, A. Lucas, O. Otto, U. F. Keyser, *Electrophoresis* **2012**, 33, 3480–3487.
- [30] R. M. M. Smeets, U. F. Keyser, D. Krapf, M. Y. Wu, N. H. Dekker, C. Dekker, *Nano Lett.* **2006**, 6, 89–95.
- [31] A. P. Ivanov, P. Actis, P. Jönsson, D. Klenerman, Y. Korchev, J. B. Edel, *ACS Nano* **2015**, 9, 3587–3594.
- [32] K. Chen, N. A. W. Bell, J. Kong, Y. Tian, U. F. Keyser, *Biophys. J.* **2017**, 112, 674–682.
- [33] S. M. Douglas, A. H. Marblestone, S. Teerapittayanon, A. Vazquez, G. M. Church, W. M. Shih, *Nucleic Acids Res.* **2009**, 37, 5001–5006.
- [34] P. Actis, A. C. Mak, N. Pourmand, *Bioanal. Rev.* **2010**, 1, 177–185.